Available online at www.sciencedirect.com
SCIENCE DIRECT®
European Journal of Mechanics B/Fluids 24 (2005) 539–554

The effect of streamwise vortices on the turbulence structure of a separating boundary layer

K.P. Angele, B. Muhammad-Klingmann

KTH, Mekanik, S-100 44 Stockholm, Sweden

Received 10 May 2004; received in revised form 29 October 2004; accepted 25 January 2005

Available online 12 April 2005

Abstract

A high Reynolds number flat plate turbulent boundary layer is investigated in a wind-tunnel experiment. The flow is subjected to an adverse pressure gradient which is strong enough to generate a weak separation bubble. This experimental study attempts to shed some new light on separation control by means of streamwise vortices with emphasize on the change in the boundary layer turbulence structure. In the present case, counter-rotating and initially non-equidistant streamwise vortices become and remain equidistant and confined within the boundary layer, contradictory to the prediction by inviscid theory. The viscous diffusion cause the vortices to grow, the swirling velocity component to decrease and the boundary layer to develop towards a two-dimensional state. At the position of the eliminated separation bubble the following changes in the turbulence structure were observed. The anisotropy state in the near-wall region is unchanged, which indicates that it is determined by the presence of the wall rather than the large scale vortices. However, the turbulence in the outer part of the boundary layer becomes overall more isotropic due to an increased wall-normal mixing and a significantly decreased production of streamwise fluctuations. The turbulent kinetic energy is decreased as a consequence of the latter. Despite the complete change in mean flow, the spatial turbulence structure and the anisotropy state, the process of transfer of turbulent kinetic energy to the spanwise fluctuating component seems to be unchanged. Local regions of anisotropy are strongly connected to maxima in the turbulent production. For example, at spanwise positions in between those of symmetry, the spanwise gradient of the streamwise velocity cause significant production of turbulent fluctuations. Transport of turbulence in the spanwise direction occurs in the same direction as the rotation of the vortices.

1. Introduction

Turbulent boundary layer separation is a flow phenomenon with great practical importance which severely affects the performance in many technical applications. The practically most common technique to control separation, on e.g. wings of commercial air-crafts, is to use Vortex Generators (VGs). These usually consist of rectangular or triangular planforms, of the order of the local boundary layer thickness, mounted normal to the surface and at an angle to the main flow direction, thereby generating streamwise vortices, see Fig. 1. The VGs can be arranged to create either co-rotating or counter-rotating vortices. The latter was used in the present study.

E-mail address: angele@thtlab.t.u.-tokyo.ac.jp (K.P. Angele).

0997-7546/$ – see front matter
doi:10.1016/j.euromechflu.2005.01.005

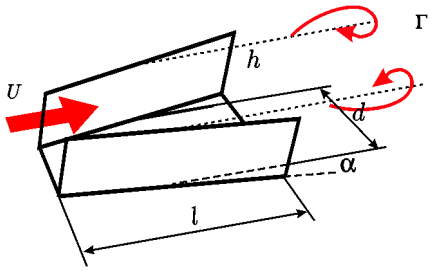

Fig. 1. The dimensions of a VG creating a pair of counter-rotating streamwise vortices in the downstream direction.

Table 1
Physical dimensions of the three different VG sets used and design criteria suggested by Pearcey [2]. $Z = 750$ mm is the spanwise width of the flat plate which means that Z/D (no.) corresponds to the number of VGs over the whole spanwise width of the plate

h (mm)	d (mm)	l (mm)	D (mm)	l/h	D/d	D/h	Z/D (no.)
10	21	30	83	3	4	8.33	9
18	37.5	54	150	3	4	8.33	5
30	62.5	90	250	3	4	8.33	3

1.1. General VG design

The relative performance of different mixing devices for separation control was already investigated by Schubauer and Spangenberg [1] in a flat plate turbulent boundary layer subjected to a strong adverse pressure gradient (APG). Mean velocity profiles were measured at different spanwise positions and spanwise averaged quantities of the displacement thickness, δ^*, and the momentum-loss thickness, θ, were compared for different pressure gradients. It was concluded that forced mixing had a similar effect as a lowering of the pressure gradient in terms of decreased values of the shapefactor, $H_{12} = \delta^*/\theta$, hence, forced mixing makes it possible to achieve a larger pressure rise in a shorter distance, i.e. to withstand a stronger pressure gradient, and delay, or perhaps even avoid, separation.

Many different VG configurations were explored by Pearcey [2] and design criteria were given for both the co-rotating and counter-rotating cases, see Table 1, for the latter. The dimensions of a VG are shown in Fig. 1 where l is the VG side length and h the height. d is the spanwise distance between two blades (at $l/2$) and D corresponds to the spanwise distance between two VGs, see Fig. 5.

Model predictions for the flow field induced by triangular wedge like VGs were made by Smith [3] to be used as a tool for VG design. The model predicted experimental data well and it was concluded that an increased benefit, in terms of increasing vortex strength, should be realized by an increased spanwise packing of VGs and by longer VGs. The most beneficial spanwise spacing was found to be $D/d = 2.4$.

The streamwise position of the VG determines the distance over which the wall shear-stress is increased, and the absolute size of the VG needed, which determines the total VG drag. More recent studies have focused on minimizing the drag caused by a VG, see the review by Lin [4]. A smaller VG gives a lower form drag and therefore submerged VGs (smaller than the boundary layer thickness) have attracted a lot of attention. Lin et al. [5] investigated submerged VGs in a separated flow over a backward facing ramp. It was found that the submerged devices with a relative height with respect to the boundary layer thickness $h/\delta = 0.1$ were effective but could not be placed more than 2δ upstream of the separation line due to a reduced downstream effectiveness.

1.2. Vortex dynamics

Pearcey [2] predicted the vortex paths, based on inviscid theory for the interaction between different vortices and the surface (the image vortices). With a counter-rotating setup, there is a transport of high momentum fluid from the free-stream towards the wall between two vortices from one VG, and there is a transport of low momentum from the wall region up towards the free-stream between the two vortices from two different VGs, see Fig. 5. For this case the following was found: initially equidistant vortices approach each other in pairs with common outflow which result in a movement away from the surface. If the vortices are arranged to be initially non-equidistant, as in Fig. 5 ($D/d \geqslant 2$), the two vortices from one VG move away from each other and towards the wall. The movement towards the wall was found to give a high maximum efficiency for separation control. However, ultimately the vortices will reach an equidistant state which will lead to a movement away from the wall. This

scenario can be delayed by increasing the relative spanwise spacing (D/h) of the VGs, thus increasing the length over which the vortices are effective, at the expense of a slightly decreased maximum efficiency. Co-rotating vortex pairs were also found to be efficient provided that the initial distance between the vortices is not too small. This will otherwise reduce their efficiency severely since the low velocity fluid lifted out from the surface by one vortex is pushed down by its neighbour. The advantage of a co-rotating vortex system is that the vortices do not move away from the surface, due to the opposite effect that the two different neighbours have on one vortex. However, the vortices are displaced laterally.

Shabaka et al. [6] and Mehta and Bradshaw [7] conducted two experiments. One on a weak single streamwise vortex and one on a weak counter-rotating vortex pair with common outflow embedded in a zero pressure-gradient (ZPG) turbulent boundary layer. In the case of the single vortex they concluded that the circulation introduced by the vortex was almost conserved and that the vortex size grows with the boundary layer in the downstream direction. The two vortices (stated to be very close to each other and to the surface initially) approached each other and moved away from the surface as predicted by the inviscid theory of Pearcey [2].

Pauley and Eaton [8] investigated both a vortex pair with common outflow and a vortex pair with common inflow. The study was carried out in a ZPG turbulent boundary layer using a VG height of approximately 150% of the local boundary layer thickness. Focus was on the downstream development of the vortices in terms of vorticity and circulation. The vortex pair with common outflow was tested for three different initial distances between the vortices: 14 cm, 10 cm and 4 cm. Only in the last case, where the distance between the vortices was smallest, they were lifted out from the surface within the test section length (200 cm). The peak vorticity associated with the vortices decreased in the downstream direction by a factor of five to six and it was observed that the circulation (the integrated vorticity) was decreased by a factor of two. For the case with common inflow, the initial VG spacing did not have any effect on the strength of the vortices but it had a strong effect on the minimum boundary layer thickness downstream of a VG. The latter was seen to decrease with decreasing initial distance between the vortices. An increase in the angle of attack did not have an effect on the minimum boundary layer thickness but the strength of the vortices increased linearly up to an angle of attack of 18°.

Zhang et al. [9] observed that pairs of counter-rotating vortices of the size of the boundary layer thickness, with common outflow, were lifted out from the surface. The vortices were initially equidistant and the distance between the vortices was approximately twice the boundary layer thickness.

Angele and Grewe [10] concluded the following for the use of VGs in control of a separating APG boundary layer. The counter-rotating vortices from one VG move away from each other in the spanwise direction and slightly outward in the wall-normal direction. The latter is contradictory to the conclusion by Pearcey [2]. The vortices had not yet become equidistant at the most downstream measurement position corresponding to $(x - x_{VG})/h = 13$. The mean size of the vortices grew with the boundary layer in the downstream direction. The maximum vorticity, associated with the vortices, decreased in the downstream direction and the vortex circulation was conserved until $(x - x_{VG})/h = 13$. Wall shear-stress measurements down to $(x - x_{VG})/h = 40$ reached an approximately two-dimensional state at $(x - x_{VG})/h = 30$. The vortices were found to be non-stationary and the movements in the spanwise direction were larger than those in the wall-normal direction, which were presumably suppressed by the wall. A correlation was found between a large instantaneous vortex size and a small maximum vorticity in the instantaneous vortex center (and vice versa) implying that the vortices are instantaneously stretched.

1.3. Vortex effect on the boundary layer turbulence structure

Shabaka et al. [6] and Mehta and Bradshaw [7] also investigated the effect of the vortices on the boundary layer turbulence structure by X-wire measurements. The normal Reynolds stresses showed large values around the vortex center and the spanwise distribution of c_f showed a sharp valley (minimum value). According to the authors these observations suggests that the spanwise wandering of the vortices is small. All the Reynolds shear stresses were found to be similar in magnitude. Regions of $-\overline{u'v'} \leqslant 0$ surrounded the vortex cores and the other Reynolds shear-stresses were anti-symmetrical in the spanwise direction with respect to the symmetry plane between the vortices. Large changes in the turbulence structural parameters, as compared to the ZPG boundary layer, were reported and the general conclusion was that simple eddy-viscosity based turbulence models are not likely to be able to predict such complicated Reynolds stress and turbulent diffusion patterns. Many other studies have observed large values of the normal Reynolds stresses around the mean vortex center, see for example Zhang et al. [9], Mehta [18] and Cutler and Bradshaw [11]. Angele and Grewe [10] coupled this to the vortex wandering.

1.4. Summary and present work

In order to optimize separation control based on streamwise vortices, we need a deeper understanding of how, why and under what conditions the vortices change the flow. In order to replace expensive experiments by numerical simulations, reliable turbulence models have to be constructed, based on a better understanding of the structural changes of the turbulence and

the underlying physics. For the calibration of such turbulence models accurate experimental data is required. With the recent development of Particle Image Velocimetry (PIV) this has become a suitable tool for this kind of measurements.

2. Method

2.1. Experimental setup

The experiments were carried out at KTH in a new closed loop wind-tunnel, Lingren and Johansson [12]. The test-section is 4.0 m long and has a cross-section area of 0.75 m $\times$ 0.5 m (z and y-directions respectively). Fig. 2 shows photographs taken inside the test-section. The first part of the test-section has a constant cross-section area, see the schematic picture displayed in Fig. 3(a), but at $x = 1.25$ m the test-section is diverged by means of a flexible wall in order to achieve a decelerating flow. Suction is applied through holes in order to prevent the boundary layer from separating on the curved surface. A flat plate mounted in

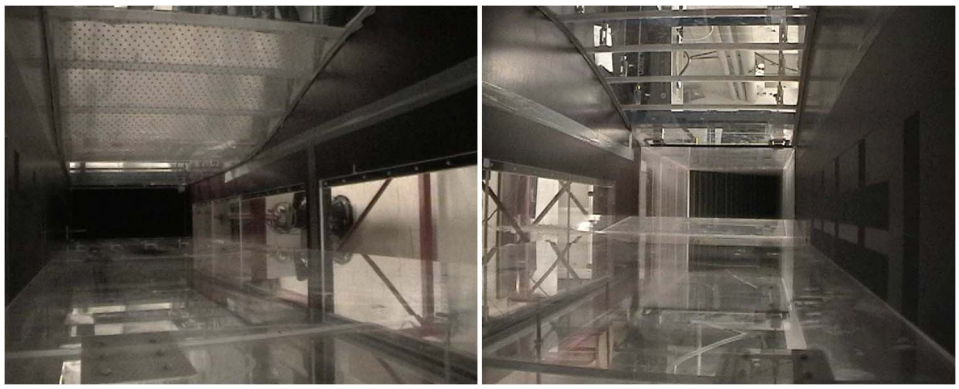

Fig. 2. The wind-tunnel test-section used in the present experiments. (a) In the upper part of the figure we see the curved surface where suction is applied and in the lower part we see the Plexiglas® flat plate where the boundary layer develops. The flow is out of the picture. (b) The flap at the downstream end of the flat plate can be seen. The flow is into the picture.

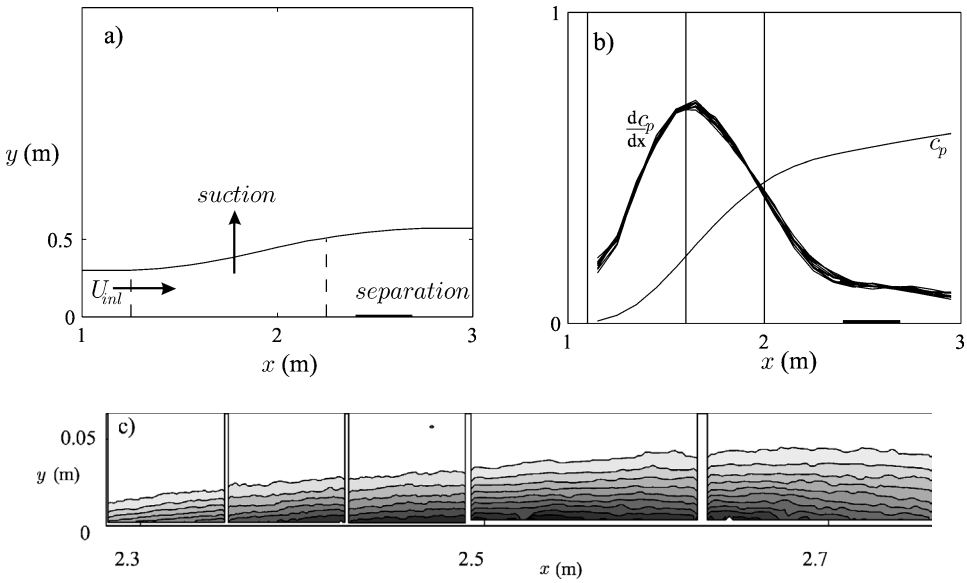

Fig. 3. (a) The geometry of the curved surface with suction applied between the vertical dashed lines. The horizontal full line indicates the extent of the separated region. (b) 10 measurements of the wall static pressure distribution and its gradient. The vertical lines show the different positions of the VGs. The horizontal full line indicates the extent of the separated region. (c) The contours of χ around the separation bubble. Each contour corresponds to an increase of 5% in χ. Note that the picture is not to scale.

the test section, is exposed to an APG using this configuration. The temperature in the test-section was kept constant at 20 °C. For a detailed description of the experimental setup and design, see Angele [13].

2.2. PIV equipment

PIV measurements were conducted with an equipment consisting of a 400 mJ double pulsed Nd:Yag laser and a digital Kodak ES1.0 CCD camera, containing 1018 × 1008 pixels. The flow was seeded by means of glycol, heated up by a smoke generator and injected through the pressure equalizer slit downstream of the test-section. This assured a homogenous seeding in the boundary layer. The camera was equipped with a Nikkor $f50$ lens and the distance between the camera and the measurement plane i.e. the laser sheet, was approximately 700 mm. The spatial resolution, using image sizes of 150 mm × 150 mm and 32 × 32 pixel PIV interrogation areas (ia), was 4.84 mm × 4.84 mm. Approximately 1000 image pairs were used for calculating the turbulence statistics. The particle image size was above 2 pixels in order to avoid serious problems with the peak-fit algorithm for sub-pixel resolution leading to peak-locking, as recommended by Westerweel [14] and Raffel et al. [15]. The light intensity is more than sufficient according to Raffel et al. [15], being approximately 6–7 bit of the 8 bit resolution. The number of particles inside each ia is above the recommended value of five, Keane and Adrian [16], to assure a good performance of the correlation technique. The overall quality of the data is high and the validation rate in the present data set is varying between 90–98%. For a general discussion on the errors induced by peak-locking, see Angele and Muhammad-Klingmann [17]. The PIV data presented here are averaged over 5–10 ias in the downstream direction.

2.3. Turbulent boundary layer separation

A separating APG turbulent boundary layer with a weak and shallow separation bubble is induced by the pressure gradient generated by the present setup. In Fig. 3(b) the downstream development of the pressure coefficient

$$c_p = \frac{P - P_{\text{ref}}}{P_0 - P_{\text{ref}}} \tag{2.1}$$

for the wall-static pressure P and its gradient in this direction is shown. The reference wall-static pressure, P_{ref}, was taken at $x = 0.45$ m in the non-diverging part of the flow and P_0 is the stagnation pressure at this position. Fig. 3(c) shows the contours of the backflow coefficient, χ, around the separation bubble. This quantity is usually used for defining the mean separation position as the one where the backflow coefficient in the vicinity of the wall, $\chi_w \geqslant 50\%$. Here it is calculated as the amount of the instantaneous PIV velocity vectors which are in the upstream direction relative to the total amount of vectors. In the present experiment $\chi_w \geqslant 50\%$ between $x = 2.4$ m and $x = 2.7$ m. The mean velocity and turbulence structure of the boundary layer around separation will be displayed in more detail in connection to the comparisons with the different cases with streamwise vortices. For detailed information about the development of the flow and the accuracy in the pressure measurements, see Angele [13].

2.4. Streamwise vortices

The streamwise vortices introduced to control the separation bubble were generated by means of VGs which create pairs of counter-rotating vortices. Table 1 shows the design criteria used here as suggested by Pearcey [2] and Fig. 1 shows the geometry of a VG. The blade angle, α, was 15°. No direct measurements of the vorticity and circulation induced by the vortices in the cross-flow (yz) plane were made, but the circulation is estimated as

$$\Gamma = \frac{Z}{D} hU, \quad U(x_{\text{VG}}, y = h) = U\big(H_{12,\Gamma=0}(x), U_\infty(x), h/\delta(x)\big) \tag{2.2}$$

where $Z = 750$ mm is the spanwise width of the flat plate and U the mean velocity at $y = h$. U is a function of the boundary layer characteristics where x_{VG} is the streamwise position of the VGs, $H_{12,\Gamma=0}$ is the shape-factor, which reflects the effect of the pressure gradient on the shape of the boundary layer velocity profile in the case without vortices. U_∞ is the local free-stream velocity and δ the local boundary layer thickness (taken as the position where the velocity reaches 99% of the free-stream velocity) at the position of the VG. The measured value of Γ in Angele and Grewe [10] is about 60% of the value when estimating the circulation like this.

By using three different VG heights at three different x_{VG}-positions, see Table 2 and Fig. 4(a), $H_{12,\Gamma=0}$, U_∞ and h/δ could be varied and Γ changed. Note that keeping all the geometric ratios listed in Table 1 constant implies that a decrease in VG height is compensated by an increase in the number of VGs (Z/D) in the spanwise direction. Fig. 4(b) shows the streamwise mean velocity profiles at the three different downstream positions where the VGs were positioned. The boundary layer thickness grows fast in the downstream direction and the free-stream velocity is decreased as the pressure gradient acts on it. The profile is loosing its fullness, which is reflected in an increase of $H_{12,\Gamma=0}$.

Table 2
Different streamwise VG positions for varying the different parameters affecting Γ

x_{VG} (m)	$\frac{2.5-x_{VG}}{h}$	$\frac{3.4-x_{VG}}{h}$	$H_{12,\Gamma=0}$	U_∞	h (mm)	h/δ	h/δ^*	Γ
1.1	78	128	1.4	26.7	18	0.95	5.4	4.7
1.6	–	60	1.6	22.7	30	0.88	3.7	3.9
1.6	50	–	1.6	22.7	18	0.53	2.2	3.3
1.6	90	–	1.6	22.7	10	0.29	1.2	2.7
2.0	17	–	2.0	20.3	30	0.50	1.7	2.7
2.0	28	–	2.0	20.3	18	0.30	1.0	2.0

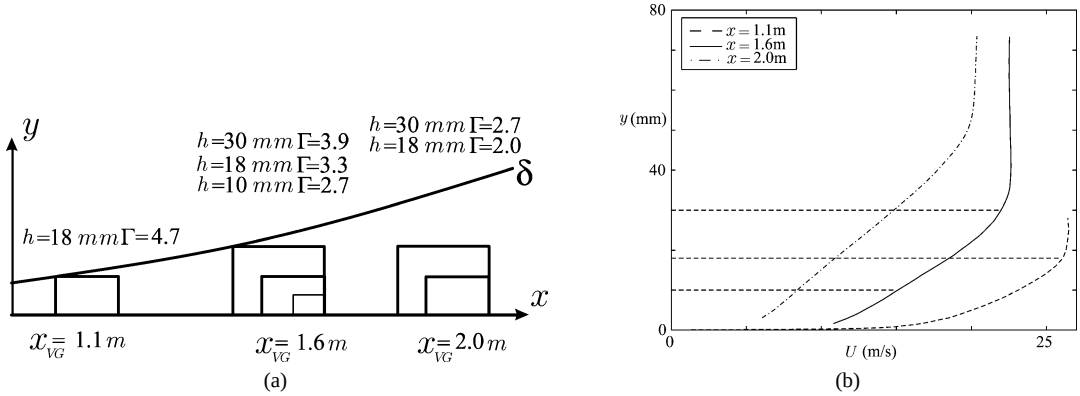

Fig. 4. (a) Downstream positions of the different VG cases. (b) The streamwise mean velocity profiles at the three different VG positions. The dashed lines corresponds to the VG heights $h = 10$ mm, $h = 18$ mm and $h = 30$ mm used in the present experiments.

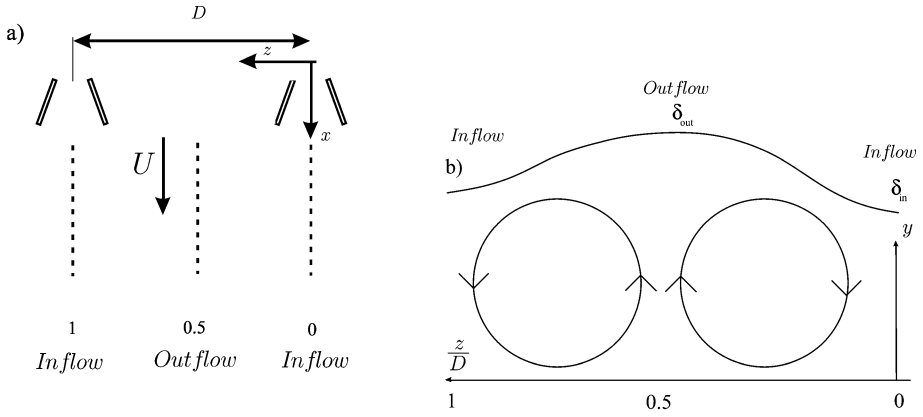

Fig. 5. (a) Two VGs seen from above. The flow is from top to bottom. (b) Schematic picture of two vortices cut in the plane of rotation once they have become equidistant. The boundary layer thickness is varying in the spanwise direction due to the successive outflow and inflow regions. The flow is out of the picture.

2.5. Measurement positions

Velocity and turbulence measurements are presented mainly for $x = 2.5$ m which corresponds approximately to the position of the maximum backflow in the case without streamwise vortices (referred to as $\Gamma = 0$), see Fig. 3(c). Some measurements will also be presented at $x = 3.4$ m to investigate the asymptotic behaviour of the vortices. Keep in mind that when VGs of different height are positioned at different streamwise positions, the vortex evolution takes place over different downstream distances. Comparison of two different cases at a fixed downstream position corresponds to different downstream development distances in terms of $(x - x_{VG})/h$, see Table 2. This implies that the vortices develop over different x-positions, i.e. subjected to slightly different pressure gradients. Downstream-spanwise xz-planes, covering the distance between two VGs at $z/D = 0$ and $z/D = 1$, see Fig. 5(a), were conducted at different wall-normal positions, and wall-normal measurements in the xy-plane

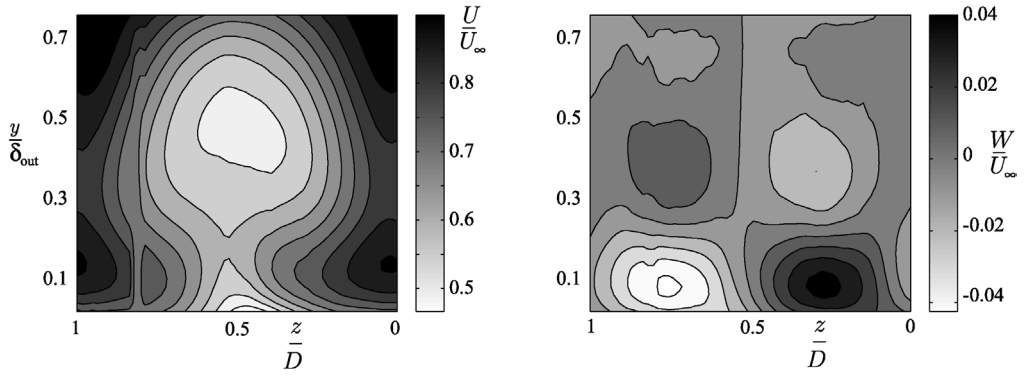

Fig. 6. PIV measurements in the xz-plane were conducted at five different wall-normal positions at $x = 2.5$ m for the case of $\Gamma = 4.7$. Positions between those, were interpolated to allow for a reconstruction of the yz-plane.

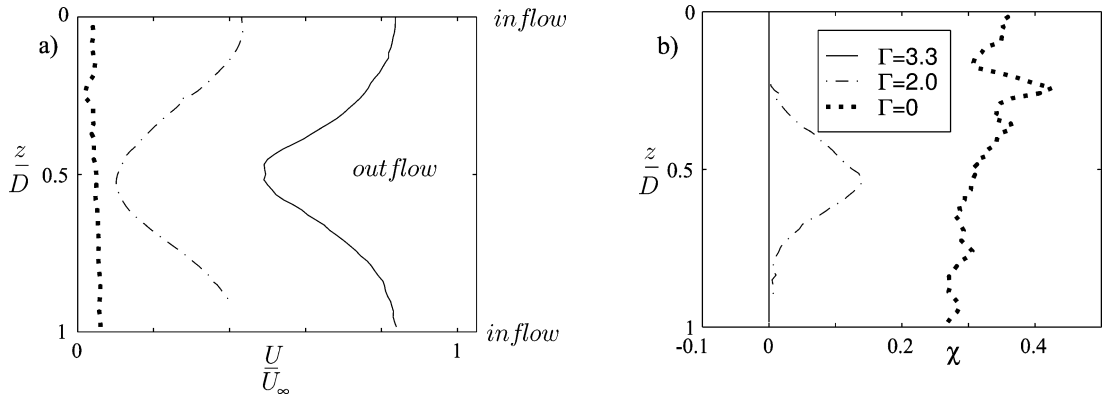

Fig. 7. (a) Mean velocity profiles in the spanwise direction at $x = 2.5$ m and $y = 10$ mm (which is below the local maximum in the wall-normal mean velocity profile, see Fig. 8(b)). (b) Variation of the backflow coefficient χ at the same position.

were conducted at different spanwise positions (preferably at $z/D = 0$ and $z/D = 0.5$, see Fig. 5(a)). These two positions are referred to as the position of *inflow* and *outflow*, respectively.

3. Results: mean flow

The contour of the streamwise velocity in the yz-plane, shown in Fig. 6(a), displays the familiar mushroom-like pattern and the vortices are easily recognized in the contour of the spanwise velocity component, shown in (b). The free-stream is not reached but one can easily imagine the variation in the boundary layer thickness in the spanwise direction from the contour of the streamwise velocity. The maximum thickness coincide with the outflow position. The mushroom-like pattern in the yz-plane is a consequence of the vortices distorting the streamlines. The vortices bring high momentum fluid towards the wall behind a VG at the inflow position. Close to the wall, this is transported by the vortices in the spanwise direction towards the region of outflow. Similarly, low momentum fluid, transported away from the wall at the position of outflow, is further transported in the spanwise direction towards the inflow regions in the outer part of the boundary layer. The spanwise velocity component is larger close to the wall than in the outer region of the boundary layer, i.e. the vortices are not symmetric. The vortex centers are approximately at $y/\delta_{\text{out}} = 0.3$ and $z/D = 0.25$ and 0.75 in the case of $\Gamma = 4.7$.

3.1. Backflow elimination

First, let us consider the effect of the streamwise vortices on the mean flow in terms of their ability to eliminate the separation. As the magnitude of backflow in separation increase towards the wall in Fig. 3(c), the changes are better observed in the near-wall region. Fig. 7(a) shows the spanwise distribution of U for two different magnitudes of Γ together with the case without vortices at $y = 10$ mm. This wall-normal position corresponds to slightly different y/δ_{out}, however, for both cases this

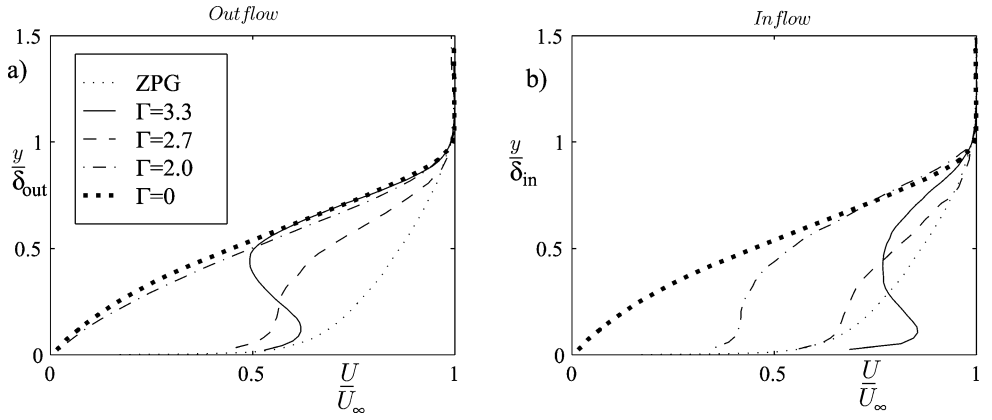

Fig. 8. Streamwise mean velocity profiles in the wall-normal direction at $x = 2.5$ m (a) at the position of outflow, $z/D = 0.5$ and (b) at the position of inflow $z/D = 0$. $\Gamma = 2.7$ refers to the case where $h/\delta = 0.29$.

corresponds to a wall-normal position of $y/\delta_{\text{out}} \leqslant 0.1$, see Fig. 8(b). The approximately two-dimensional dotted line indicates the case without vortices. The mushroom-shaped contour of the streamwise velocity in the yz-plane becomes a wake-like profile when viewed in the xz-plane. The same wake-like 3D structure can be seen in both cases with VGs, however, the profile for the lowest amount of circulation differs in that the overall level of U is lower and closer to the case without vortices. The spanwise variation of the backflow coefficient, χ, extracted from the same data, is shown in Fig. 7(b). The case without vortices has a backflow coefficient of approximately 0.3. For the case with the smallest circulation, instantaneous backflow occurs, with a maximum at the spanwise position of outflow. The amount of backflow is decreasing towards the inflow positions and right downstream of the VGs the backflow is locally eliminated. The fact that the flow is locally attached at the positions of inflow is probably reducing strong instantaneous three-dimensionality inherent in separation. When increasing the circulation, the backflow is eliminated at all spanwise position and in the present case separation is prevented for $\Gamma \geqslant 2.7$.

Fig. 8 shows the wall-normal profiles $U(y)$ at the positions of outflow (a) and inflow (b) respectively. In the case without vortices the profile is similar to a mixing layer profile. The mushroom-shaped contour of the streamwise velocity in the yz-plane becomes an S-shaped profile when viewed in the xy-plane. As noted in connection to Fig. 7(b), the position of outflow is the most sensitive in terms of separation prevention whereas the inflow position is the least sensitive. The case with the lowest amount of circulation does not change the mean velocity profile much at the position of outflow, however, at the position of inflow, the profile is changed and the flow is locally attached as was seen in Fig. 7(b). For $\Gamma = 3.3$ the shape of the velocity profile in the wall-normal direction is drastically changed at *both* the inflow and outflow positions. At the position of outflow, the outer part of the mean velocity profile is similar to the case without vortices while the near-wall gradient is strongly enhanced with a similar magnitude as for a ZPG boundary layer (only shown for comparison). Between the inner and outer regions in the wall-normal direction there is a middle region with a negative velocity gradient. For the case in between the two former, $\Gamma = 2.7$ ($h/\delta = 0.29$), the velocity profiles are not as full and strongly S-shaped as in the case of $\Gamma = 3.3$, however, the flow is attached at all spanwise positions.

Fig. 9(a) shows the boundary layer thickness at the two positions of inflow and outflow. The boundary layer with vortices is overall thicker and the outflow position is thicker than the inflow position. The boundary layer thickness is increasing with circulation and there is a drastic change between $\Gamma = 2.0$ and $\Gamma = 2.7$, which is strongly correlated with the ability of preventing separation. Fig. 9(b) shows the shape factor at the two positions of inflow and outflow. The velocity profiles are fuller at the position of inflow, i.e. it has a lower value of the shape factor, and the outflow position is the least favorable position from the point of view of flow attachment. The shape factor is decreasing with circulation and, again, there is a drastic change between $\Gamma = 2.0$ and $\Gamma = 2.7$, which is strongly correlated with the ability of preventing separation. For $\Gamma \geqslant 2.7$, there is little change in the shape-factor.

3.2. Vortex dynamics

The vortices grow in size with the growing boundary layer in the downstream direction and are hence subject to viscous and turbulent diffusion. Let us consider the effect of varying the relative VG height and the streamwise position on the shape of the velocity profile at a fix downstream position. Fig. 9(c) shows $U(y)$ at the outflow position at $x = 2.5$ m for three different values of h/δ. The cases of $\Gamma = 4.7$ and 3.9, differ in the absolute VG size and the position where the vortices are introduced while h/δ is of similar magnitude, see Table 2 and Fig. 4(a). The profiles have local maxima and minima in the S-shaped mean

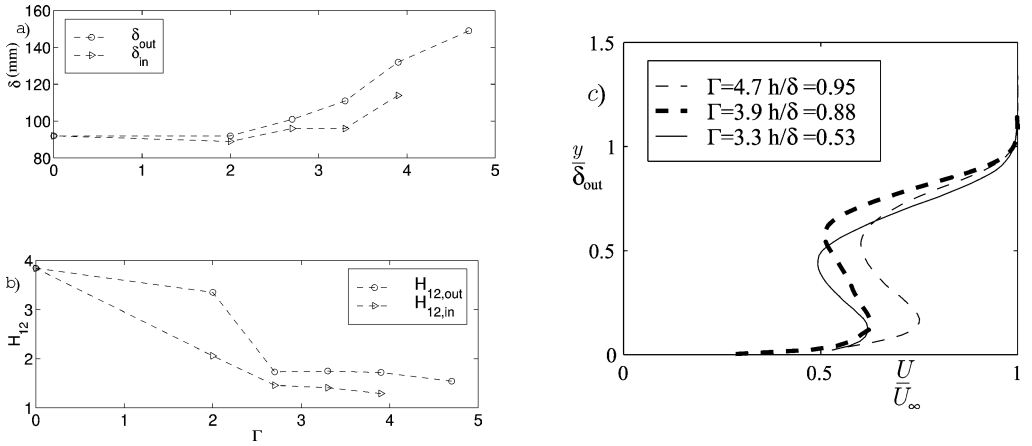

Fig. 9. The effect of the streamwise vortices on the boundary layer parameters at $x = 2.5$ m. $\Gamma = 2.7$ refers to the case where $h/\delta = 0.29$. (a) The boundary layer thickness (b) the shapefactor. (c) Streamwise mean velocity profiles in the wall-normal direction at $x = 2.5$ m and the position of outflow as a function of the relative VG height.

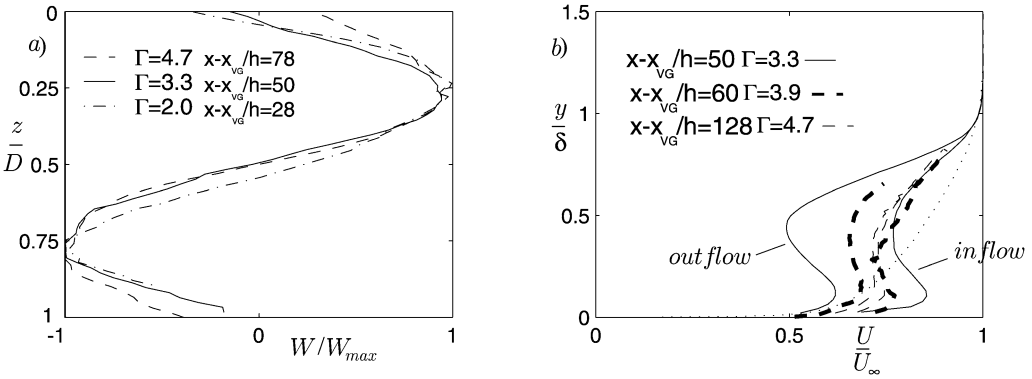

Fig. 10. (a) Mean spanwise velocity profiles at $y = 10$ mm, $x = 2.5$ m and (b) the downstream development of the mean streamwise velocity in the wall-normal direction at the positions of outflow and inflow. The dotted line corresponds to a ZPG mean velocity profile for comparison.

velocity profiles at approximately the same wall-normal positions, indicating that the vortices are similar in size. In the cases of $\Gamma = 3.9$ and 3.3, the vortices are introduced at the same streamwise position but the VG height is varied. Comparing these two mean velocity profiles, the S-shaped part of the profile is closer to the wall in the case of a relatively smaller VG, i.e. for a relatively smaller VG a smaller vortex is obtained. In Fig. 8 one can note that the cases of $\Gamma = 2.7$ and 2.0, where $h/\delta = 0.3$ approximately, are similar and display S-shaped mean velocity profiles which are even closer to the wall. Note that in $\Gamma = 3.9$, 3.3 and 2.7, separation was eliminated despite that h/δ is changed from 0.88, 0.53 to 0.29 by varying the absolute size of the VG at the same streamwise position.

In the present case the vortices are initially non-equidistant and develop towards an equidistant state further downstream. This can be seen from the fact that the maxima in $W(z)$, which correspond to the vortex center positions, are positioned at $z/D = 0.25$ and 0.75, see Fig. 10(a). It can be seen that the vortices are equidistant at $(x - x_{\mathrm{VG}})/h \geqslant 28$ in the case of $\Gamma = 2.0$. Since all the cases displayed are equidistant and corresponds to different values of $(x - x_{\mathrm{VG}})/h$, this suggests that once the vortices have become equidistant, they remain so. The VGs should be position far enough upstream of the separation in terms of $(x - x_{\mathrm{VG}})/h$ in order for the vortices to become equidistant to avoid pockets of backflow. In the case of $\Gamma = 2.7$ and $h/\delta = 0.50$, the vortices are not yet equidistant at $x = 2.5$ m which corresponds to $(x - x_{\mathrm{VG}})/h = 17$. The measurements, displayed in Fig. 10(b), show the wall-normal velocity profiles at $(x - x_{\mathrm{VG}})/h = 50 - 128$. It can be seen that, as $(x - x_{\mathrm{VG}})/h$ increases, the two profiles at the different spanwise positions of inflow and outflow approach each other, i.e. the boundary layer develops towards a two-dimensional state. The dotted line, corresponding to a ZPG mean velocity profile, is only shown for comparison to illustrate the significant change in the shape of the streamwise mean velocity profile. It can be seen that the mean velocity profiles close to the wall are fuller than in the ZPG case.

In the present case, once equidistant, the vortices remain so and are confined within the boundary layer, contradictory to the inviscid theory. The magnitude of the inviscid effect decrease with increasing spanwise spacing between two vortices and with a decrease in the magnitude of the swirling component. Pauley and Eaton [8] showed that the initial distance between the vortices with common outflow had to be small enough for the vortices to be lifted out from the surface within the wind-tunnel test-section. Mehta and Bradshaw [7] and Zhang et al. [9] also observed that tightly spaced vortex pairs with common outflow were lifted out from the surface. The vortices are also subjected to the viscous diffusion in the boundary layer which cause them to grow in size in the downstream direction as was observed by Mehta and Bradshaw [7] and Angele and Grewe [10]. Inviscid theory can not predict this growth and the accompanying decrease in the magnitude of the swirling components observed by Angele and Grewe [10]. The boundary layer thickness in APG is growing more rapidly than in ZPG in the downstream direction case, which enhance this effect.

4. Results: turbulence

4.1. The Reynolds stresses

Let us consider the yz-plane contours of the Reynolds stresses, displayed in Fig. 11. All the Reynolds stresses have a similar pattern with two distinct maxima in the middle of the boundary layer around at $y/\delta_{\text{out}} = 0.5$ and $z/D = 0.2$ and 0.8, symmetric with respect to the position of outflow (the Reynolds shear-stress is antisymmetric). Note that, these positions do not coincide with the vortex centers at $y/\delta_{\text{out}} = 0.3$ and $z/D = 0.25$ and 0.75 and hence are not induced by wandering of the vortices as was noted in the near-field of a VG by Angele and Grewe [10]. The normal stresses $\overline{u'^2}$ and $\overline{w'^2}$, also have a peak at the position of outflow in the outer part of the boundary layer. This is slightly difficult to see here since not the whole boundary layer is captured. The ratio between $\overline{u'^2}$ and $\overline{w'^2}$ is also displayed. The components are of similar magnitude around the symmetry

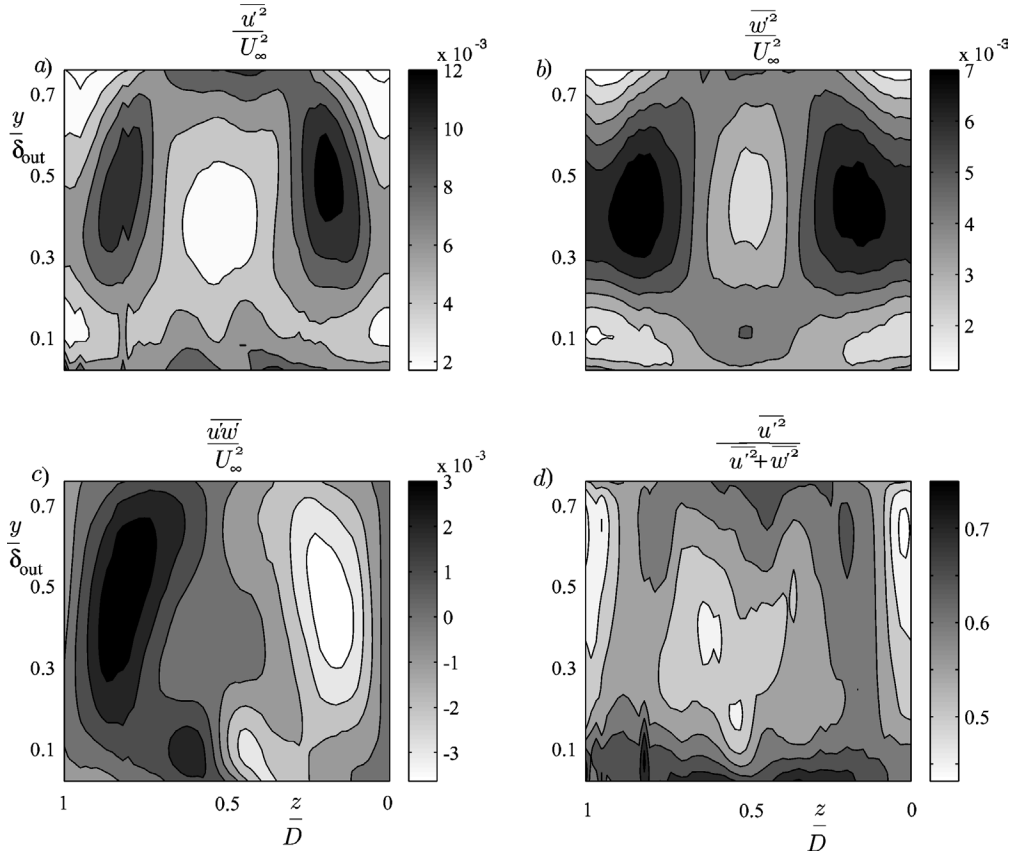

Fig. 11. Reconstruction of the Reynolds stresses in the yz-plane by interpolation of the data in the xz-planes at $x = 2.5$ m for $\Gamma = 4.7$.

positions of inflow and outflow outside the near-wall region. In the near-wall region and around the positions of maxima in $\overline{u'^2}$ and $\overline{w'^2}$ the former becomes relatively larger.

It is instructive to consider $\overline{u'w'}$. For counter-rotating vortices, $\partial U/\partial z$ changes sign at the spanwise position of outflow, which gives an asymmetry around this position, as was noted by Mehta and Bradshaw [7]. At the outflow and inflow regions $\partial U/\partial z$ vanishes. The behaviour of $\overline{u'w'}$ can be interpreted in the same way as $-\overline{u'v'}$ caused by the wall-normal gradient in U in a two-dimensional boundary layer, since $\overline{u'w'}$ reflects turbulent transport of momentum in the spanwise direction. Consider the vortex with center at $z/D = 0.75$ where $\overline{u'w'} \geqslant 0$. Below the vortex center (i.e. close to the wall), high momentum fluid ($u' \geqslant 0$) is carried along the wall towards the position of outflow in the positive spanwise direction (i.e. $w' \geqslant 0$). Above the vortex center (close to the free-stream), low momentum fluid ($u' \leqslant 0$) is carried away from the position of outflow in the negative spanwise direction (i.e. $w' \leqslant 0$) and consequently $\overline{u'w'} \geqslant 0$ throughout the boundary layer in the wall-normal direction. The magnitude of $\overline{u'w'}$ is similar to that of $-\overline{u'v'}$ which indicates its significance. Due to the mushroom-like structure in the yz-plane contour of the streamwise velocity, the wake-like structure in an xz-plane has inflection points at different spanwise positions depending on the wall-normal position of consideration. Close to the wall, the wake-like profile is narrower and the inflection points are closer to the position of outflow. The inflection points are crucial for the turbulence production, as we will see in next section, which explains why the Reynolds shear stress maxima moves closer to the position of outflow when approaching the wall.

4.2. The production of turbulence

The turbulence production is defined as

$$P_{ij} = -\overline{u_i' u_k'}\frac{\partial U_j}{\partial x_k} - \overline{u_j' u_k'}\frac{\partial U_i}{\partial x_k}. \tag{4.1}$$

The two major effects of the vortices on the mean flow which influence the turbulence structure are the wake-like structure in the spanwise direction, and the S-shaped streamwise mean velocity profiles in the wall-normal direction, i.e., the dominating gradients are $\partial U/\partial y$ and $\partial U/\partial z$. The major production terms are therefore

$$P_{uu} = P_{uu}^{\mathrm{I}} + P_{uu}^{\mathrm{II}} = -\overline{u'v'}\frac{\partial U}{\partial y} - \overline{u'w'}\frac{\partial U}{\partial z}, \tag{4.2}$$

$$P_{uv} = P_{uv}^{\mathrm{I}} + P_{uv}^{\mathrm{II}} = -\overline{v'v'}\frac{\partial U}{\partial y} - \overline{v'w'}\frac{\partial U}{\partial z}, \tag{4.3}$$

$$P_{uw} = P_{uw}^{\mathrm{I}} + P_{uw}^{\mathrm{II}} = -\overline{w'v'}\frac{\partial U}{\partial y} - \overline{w'w'}\frac{\partial U}{\partial z}. \tag{4.4}$$

P_{vv}, P_{vw} and P_{ww}, i.e. production of $\overline{v'^2}$, $\overline{v'w'}$ and $\overline{w'^2}$, are induced by gradients in the secondary flow components V and W which are comparatively small. With the present PIV measurements in the xz-plane we have access to P_{uu}^{II} and P_{uw}^{II} and from the xy-plane measurements we get P_{uu}^{I} and P_{uv}^{I}.

It is instructive to consider positions where the turbulence is locally governed by one of the two gradients. Fig. 12 (a) and (b) display opposite trends in the spanwise structure of $\overline{u'^2}$ and $\overline{w'^2}$. Different quantities are displayed side by side to allow for a visual impression of the correlation between them. Gains and offsets used for the different parameters are displayed in Table 3. In (b) $\partial U/\partial y$ is locally zero at the position of outflow, see Fig. 9(c), and the turbulence is locally governed by $\partial U/\partial z$. This is evident as the maxima of the Reynolds stresses coincide with the maxima in their respective production terms P_{uu}^{II} and P_{uw}^{II}. In (a) instead, the positions of the maxima in the Reynolds stresses are not correlated with the maxima in the production terms, but are instead located at the outflow region, where $\partial U/\partial z$ is zero. This indicates that the turbulence is now governed by $\partial U/\partial y$ which has a local maximum, see Fig. 9(c).

At the outflow and inflow regions the spanwise gradient vanish and the production is governed by the wall-normal velocity gradient. The production terms $P_{uu}^{\mathrm{I}} = P_{uu}$ and $P_{uv}^{\mathrm{I}} = P_{uv}$ and the flow is quasi-two dimensional. This makes this position suitable for a direct comparison with the case without vortices. Fig. 13(a)–(d) is organized in the same way as Fig. 12, allowing for a direct comparison of the different components and their magnitude. In the case without vortices there is a single production peak in the middle of the boundary layer. This is a typical feature of APG boundary layers, see Angele [13]. In the controlled

Table 3
Gains and offsets used for the different parameters displayed in Figs. 12 and 13

$\overline{u_i' u_j'}$	P_{ij}	U	$\partial U/\partial x_j$
$10^3/U_\infty^2$	$\delta/U_\infty^3 + 15$	2	$-10^2\delta/U_\infty$

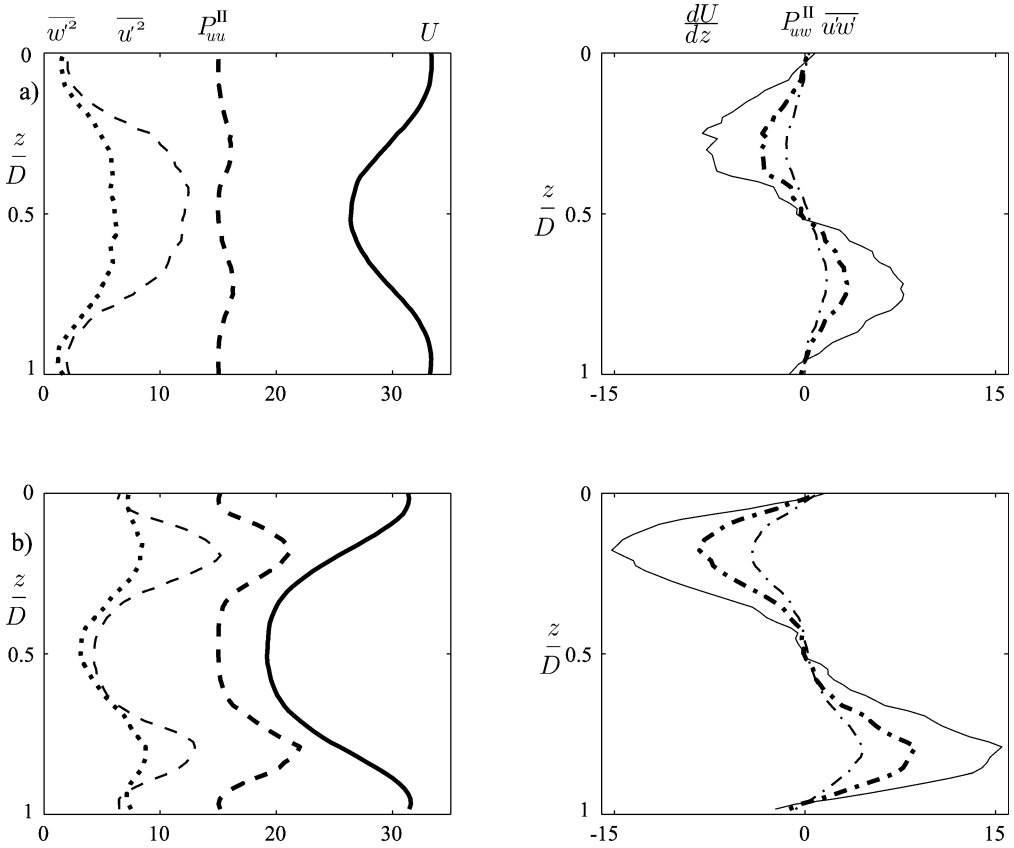

Fig. 12. The turbulence structure in the xz-plane in the case of $\Gamma = 4.7$ at the wall-normal positions: (a) $y/\delta_{\mathrm{out}} = 0.76$ and (b) $y/\delta_{\mathrm{out}} = 0.52$.

case, P_{uu}^{I} and P_{uv}^{I} have peaks of similar magnitude as the case without vortices but instead in the outer region and close to the wall induced by the large mean velocity gradient in the S-shaped velocity profile. This causes maxima in $\overline{u'^2}$ (as was also seen in Fig. 12(a)) and $-\overline{u'v'}$ at approximately the same wall-normal positions. In the middle of the boundary layer, P_{uu} is approximately zero, which gives overall lower values of $\overline{u'^2}$. P_{uv}^{I} in the middle region is negative, i.e. we have a destruction of the Reynolds shear-stress, which results in negative values of $-\overline{u'v'}$ itself, as was noted by Mehta and Bradshaw [7]. In the controlled case we have a significantly lower magnitude of streamwise fluctuations in the middle of the boundary layer due to the absence of production. As opposed to that, the wall-normal fluctuations are slightly larger in the controlled case which makes them comparable in magnitude to the streamwise fluctuations. The ratio between $\overline{u'^2}$ and $\overline{v'^2}$ is similar to that of $\overline{u'^2}$ and $\overline{w'^2}$, see Fig. 12.

4.3. Turbulent kinetic energy and the anisotropy state

The relative magnitude of the different components in the Reynolds stress tensor is expressed by the anisotropy tensor

$$a_{ij} = \frac{\overline{u_i' u_j'}}{k} - \frac{\delta_{ij}}{3}, \quad k = \frac{1}{2}\left(\overline{u_k' u_k'}\right), \tag{4.5}$$

where δ_{ij} is the Kronecker-delta and k the turbulent kinetic energy. Figs. 14(a)–(d) show the components of the anisotropy tensor which are non-zero at the position of outflow, a_{11}, a_{22}, a_{33} and a_{12}. Close to the wall the anisotropy components are similar, which indicates that the anisotropy state in this region is determined by the presence of the wall rather than the large scale vortices. Outside the near-wall region the a_{11} component has a lower value which is closer to zero, i.e. more isotropic, and a_{22} has a higher value which is closer to zero, for the controlled case. a_{33} is virtually unchanged. The a_{11} component is decreased due to the absence of production of turbulence and the a_{22} component is increased, due to an increased wall-normal mixing. The fact that the a_{33} component is unchanged suggests that the process of turbulence transfer which feeds energy into

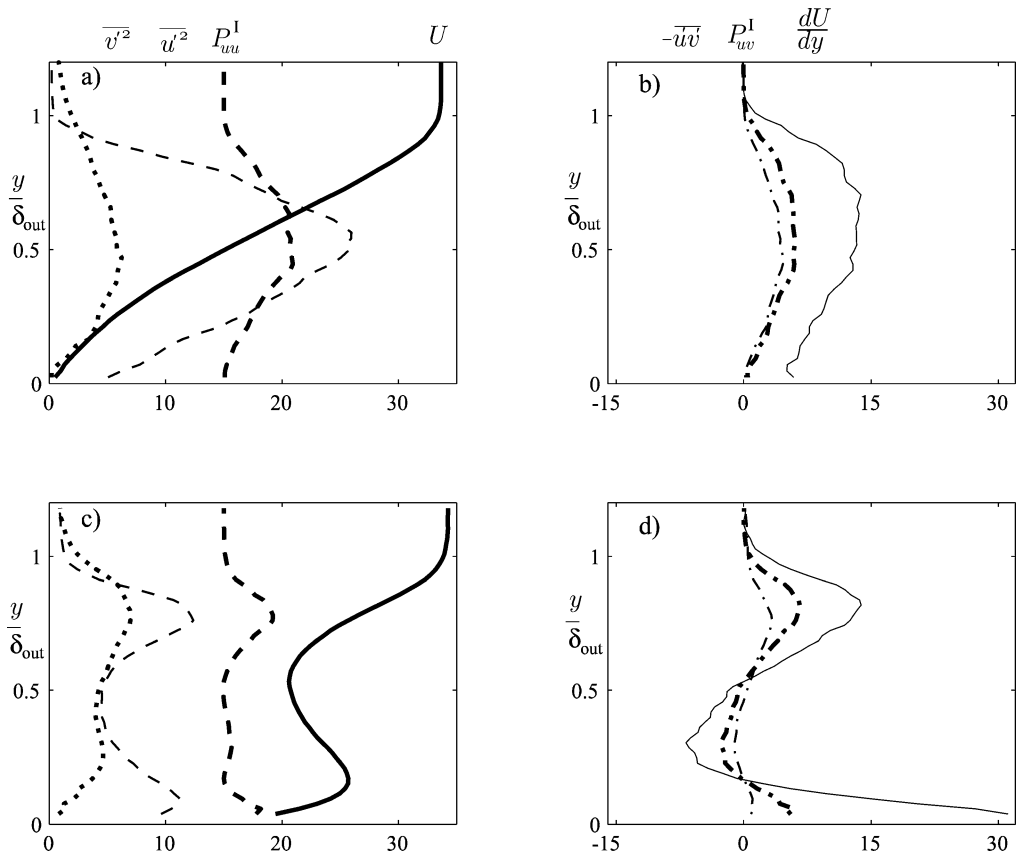

Fig. 13. The turbulence structure in the wall-normal direction at the spanwise position of outflow for the case without vortices $\Gamma = 0$ (a, b) and for the case of $\Gamma = 4.7$ (c, d).

the a_{33} component is undisturbed by the presence of the vortices even though the mean flow and the total anisotropy state itself is very much changed by the vortices.

Fig. 15(a) shows the relative magnitude of the streamwise and the wall-normal fluctuations at four spanwise positions. For all these spanwise positions the two components are more similar than in the case without vortices. This leads to the conclusion that the turbulence in the outer region is overall more isotropic than the case without vortices, since the relative magnitude between the streamwise and the spanwise fluctuations display the same behavior in the outer region, see Fig. 11(d). The wall-normal and spanwise positions where the streamwise fluctuations become relatively large in comparison with the other components are strongly connected to maxima in P_{uu}^{I} and P_{uu}^{II}, see Figs. 12(b) and 13(c). Also, the positions where the production vanish, such as in the middle region of the boundary layer at the symmetry position of outflow, the ratio between all the stresses is approximately one and the turbulence is isotropic.

Concerning the overall level of the turbulent fluctuations, Fig. 15(b) shows that, at the position of outflow, through out the middle region of the boundary layer, the turbulent kinetic energy has a lower magnitude in the controlled case, due to the vanishing turbulent production. As a consequence, the value of the integrated turbulent kinetic energy in the wall-normal direction, at the position of outflow, is lower than in the case without vortices. As is shown in Fig. 16(b), the production in the outer region is even lower at the position of inflow which makes the turbulent kinetic energy even lower. In the cross-flow region, relatively high levels of turbulence is associated with production due to the spanwise gradients, however, the level of the fluctuations is still smaller in magnitude than in the case without vortices and the total turbulent kinetic energy is consequently lower.

Comparing P_{uu}^{I} in the cases where $\Gamma \geqslant 3.3$ at $x = 2.5$ m, the maximum values in the outer region, at the spanwise position of outflow, increase with decreasing circulation, see Fig. 16(a). This can be explained by the fact that with increasing circulation, δ_{out} at $x = 2.5$ m increase, see Fig. 9(a), and the velocity gradient, and thereby the production, decrease since the free-stream velocity at $x = 2.5$ m is the same. Since an increasing anisotropy is correlated with this outer maxima in the production, the outer region becomes more isotropic with increasing circulation. The near-wall region shows the opposite trend for the production,

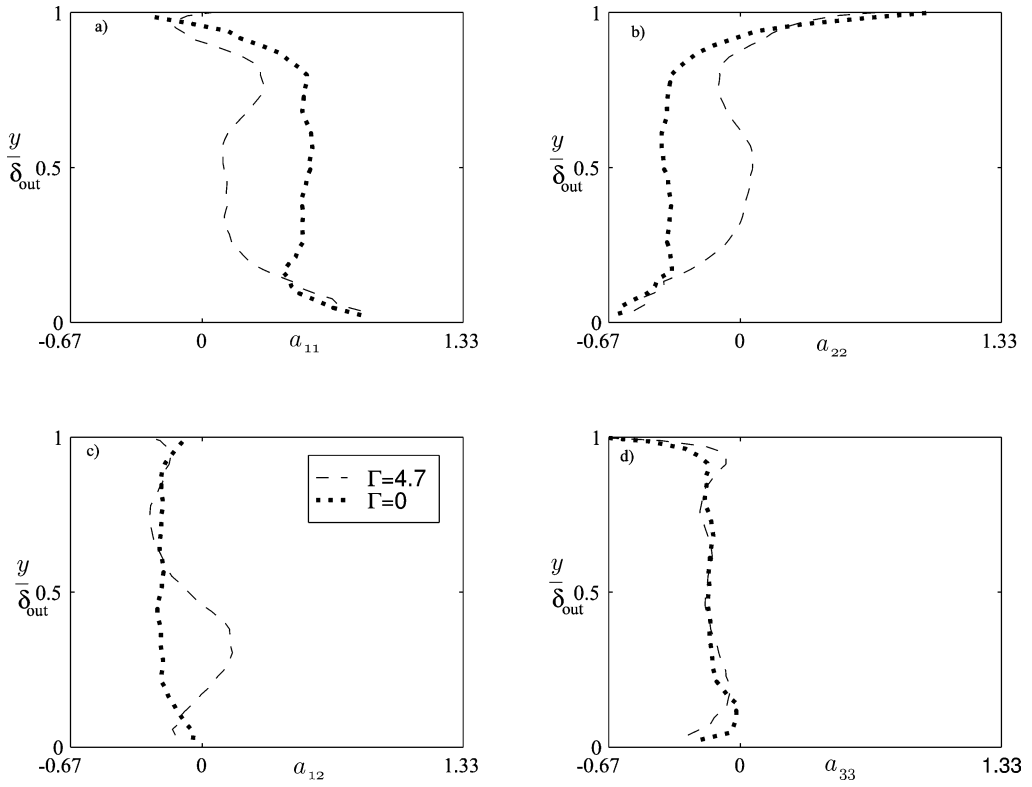

Fig. 14. The wall-normal structure of the anisotropy components which are non-zero at the spanwise position of outflow for $\Gamma = 4.7$ and 0 at $x = 2.5$ m.

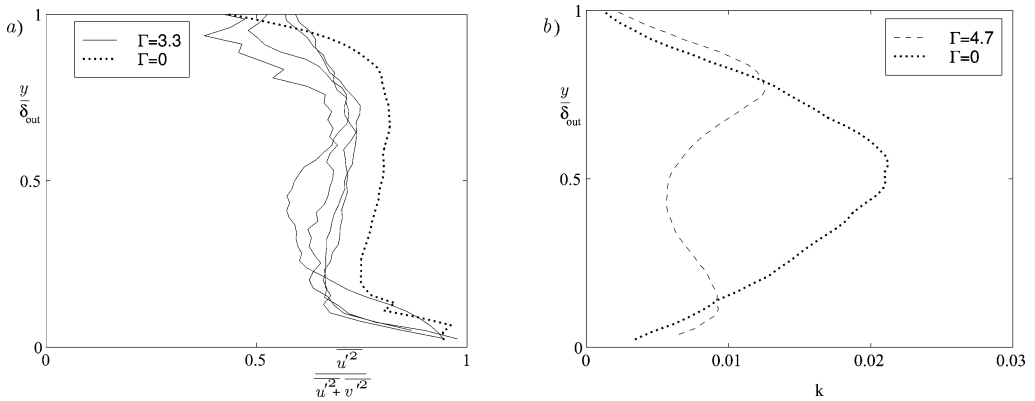

Fig. 15. (a) The relative magnitude of the streamwise and the wall-normal fluctuations at $x = 2.5$ m for $\Gamma = 3.3$ at $z/D = 0$, 0.125, 0.25 and 0.5 compared to $\Gamma = 0$. (b) The turbulent kinetic energy, k at the spanwise position of outflow at $x = 2.5$ m.

and the magnitude increases with increasing circulation. Fig. 16(b) compares the production for the positions of outflow and inflow. The two positions display the opposite behavior in the magnitude of the outer and the near-wall peaks, which can be explained by the magnitude of $\partial U/\partial y$, see Fig. 10(b). This leads to the conclusion that the outer region at the position of inflow is more isotropic than the outer region at the position of outflow.

5. Summary and conclusions

A separating adverse pressure gradient turbulent boundary layer was controlled by means of streamwise vortices in a wind-tunnel experiment. PIV was used to investigate the change in the meanflow and the turbulence structure. Measurements were

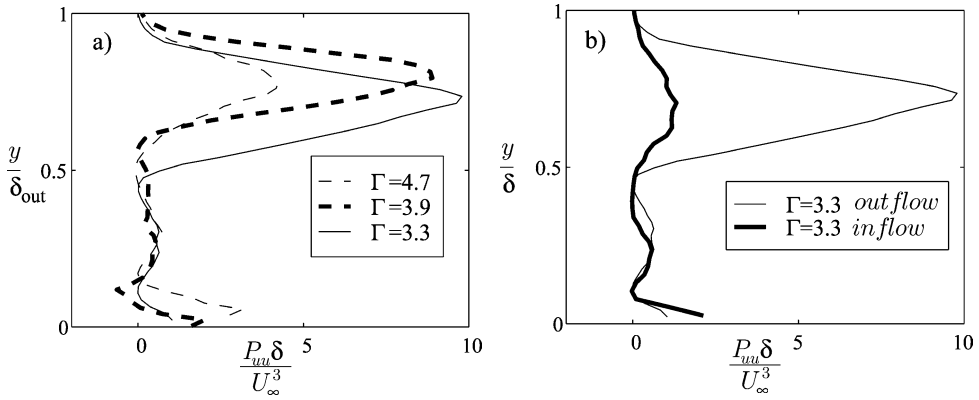

Fig. 16. The turbulence production P_{uu}^{I} (a) for $\Gamma \geqslant 3.3$ for the spanwise position of outflow at $x = 2.5$ m and (b) for the different spanwise positions of inflow and outflow for $\Gamma = 3.3$ at $x = 2.5$ m.

concentrated to the downstream position where a separation bubble is present in the case without vortices and focus is on the change in the turbulence structure. The viscous diffusion cause the vortices to grow, the swirling velocity component to decrease and the boundary layer to develop towards a two-dimensional state. Counter-rotating and initially non-equidistant streamwise vortices become and remain equidistant and confined within the boundary layer, contradictory to the prediction by inviscid theory. At the position of the former separation bubble we could observe a fuller velocity profile close to the wall and an increased production in the near-wall region when the circulation was increased. At the symmetry positions of inflow and outflow the gradients in the spanwise direction vanish. The middle part of the boundary layer in the wall-normal direction has no production of streamwise fluctuations and there is a destruction of the Reynolds shear-stress. As a consequence of this, the total turbulent kinetic energy is lower than in the case without vortices. In the near-wall region, the anisotropy state is unchanged which indicates that it is determined by the presence of the wall rather than the large scale vortices. However, the flow outside the near-wall region becomes more isotropic due to an increased wall-normal mixing and the absence of turbulent production. The a_{33} component is unchanged which suggests that the process of transfer of turbulent kinetic energy to the spanwise component is unchanged despite the complete change in the mean flow, the turbulence structure and the anisotropy state. Local regions of anisotropy are strongly connected to production maxima. At spanwise positions between those of inflow and outflow, the spanwise gradient of the streamwise mean velocity causes significant levels of turbulence production, however, the flow is overall more isotropic. Transport of turbulence in the spanwise direction occur in the same direction as the rotation of the vortices.

Acknowledgements

Special thanks are owed to Dr. Björn Lindgren, Lic. Olle Törnblom, Dr. Fredrik Lundell and Dipl. Ing. Frank Grewe for valuable comments on the manuscript, Markus Gällstedt and Ulf Landén for their skilled work-shop assistance, Kyle Mowbray for assembling the test-section and finally Dipl. Ing. Frank Grewe, Ola Lögdberg and Toshiaki Kenchi, for participating during some of the measurements. This project was funded by The Swedish Research Council.

References

[1] G. Schubauer, W. Spangenberg, Forced mixing in boundary layers, J. Fluid Mech. 8 (1960) 10–32.
[2] H.H. Pearcey, Shock-induced separation and its prevention by design and boundary-layer control, in: G.V. Lachmann (Ed.), Boundary Layer and Flow Control, its Principle and Applications, vol. 2, Pergamon Press, Oxford, England, 1961.
[3] F.T. Smith, Theoretical prediction and design for vortex generators in turbulent boundary layers, J. Fluid Mech. 270 (1994) 91–131.
[4] J.C. Lin, Review of research on low-profile vortex generators to control boundary-layer separation, Prog. Aerospace Sci. 38 (2000) 389–420.
[5] J. Lin, F. Howard, G. Selby, Turbulent flow separation control through passive techniques, AIAA Paper 89-0976, 1989.
[6] I.M.M.A. Shabaka, R.D. Mehta, P. Bradshaw, Longitudinal vortices imbedded in turbulent boundary layers. Part 1. Single vortex, J. Fluid Mech. 155 (1985) 37–57.
[7] R.D. Mehta, P. Bradshaw, Longitudinal vortices imbedded in turbulent boundary layers. Part 2. Vortex pair with “common flow” upwards, J. Fluid Mech. 188 (1988) 529–546.

[8] W.R. Pauley, J.K. Eaton, Experimental study of the development of longitudinal vortex pairs embedded in a turbulent boundary layer, AIAA J. 26 (7) (1988) 816–823.
[9] H. Zhang, X. Zhang, D. Hurst, M.W. Collins, An LDA study of longitudinal vortices embedded in a turbulent boundary layer, in: 8th International Symposium Applications of Laser Techniques to Fluid Mechanics, 1996.
[10] K. Angele, F. Grewe, Investigation of the development of streamwise vortices from vortex generators in APG separation control using PIV, in: 11th International Symposium Applications of Laser Techniques to Fluid Mechanics, 2002.
[11] A. Cutler, P. Bradshaw, Vortex/boundary layer interaction, AIAA Paper 89-0083, 1989, pp. 1–11.
[12] B. Lindgren, A.V. Johansson, Evaluation of a new wind-tunnel with expanding corners, Exp. Fluids 36 (2004) 197–203.
[13] K. Angele, Experimental studies of turbulent boundary layer separation and control, PhD thesis, Dept. Mechanics, Royal Institute of Technology, Stockholm, 2003.
[14] J. Westerweel, Fundamentals of digital particle image velocimetry, Meas. Sci. Technol. 8 (1997) 1379–1392.
[15] M. Raffel, C. Willert, J. Kompenhans, Particle Image Velocimetry. A Practical Guide, Springer-Verlag, 1998.
[16] R. Keane, R. Adrian, Theory of cross-correlation in PIV, Appl. Sci. Res. 49 (1992) 191–215.
[17] K. Angele, B. Muhammad-Klingmann, A simple model for the effect of peak-locking on the accuracy of boundary layer turbulence statistics in digital PIV, Exp. Fluids, in press.
[18] R.D. Mehta, Effect of a longitudinal vortex on a separated turbulent boundary layer, AIAA Paper 85-0530, 1985, pp. 1–11.